JAST, Vol. 4, No. 3, pp 13–24

JAST
Journal of Aerospace Science and Technology

Maximum Allowable Dynamic Load of Flexible 2-Link Mobile Manipulators Using Finite Element Approach

M. H. Korayem[1], A. Heidari[2], A. Nikoobin[3]

In this paper a general formulation for finding the maximum allowable dynamic load (MADL) of flexible link mobile manipulators is presented. The main constraints used for the algorithm presented are the actuator torque capacity and the limited error bound for the end-effector during motion on the given trajectory. The precision constraint is taken into account with two boundary lines in plane which are equally offset due to the given end-effector trajectory, while a speed-torque characteristics curve of a typical DC motor is used for applying the actuator constraint. Finite element method (FEM) is utilized for deriving the kinematic and dynamic equations which considers the full nonlinear dynamic of mobile manipulator. In order to verify the effectiveness of the presented algorithm, two simulation studies considering a flexible two-link planar manipulator mounted on a mobile base are presented and the results are discussed.

INTRODUCTION

Flexible mobile robot manipulator systems exhibit many advantages over their traditional rigid arm counterparts; they require less material, have less arm weight, consume less power, are more maneuverable, require smaller actuators and are more transportable. Due to their extended workspace, mobile manipulators offer an efficient application for wide areas. But these systems are usually "power on board" with limited capacity. Hence, using light and small platforms and motor actuators in order to minimize the inertia and gravity effects on actuators will help a mobile manipulator to work in an energy-efficient manner. Using smaller actuators reduces the torque capacity of the actuators and limits the capability of carrying heavy loads.

Flexible robot manipulator has a growing application in aerospace. Light weight and easy shipping to the space is one of the advantages of these kinds of robots. On the other hand, rigid assumption for modeling the long arm manipulators which are used in space for assembling the space state will be inaccurate. Light weight and easy shipping to the space (less fuel), usage of longer arm manipulator in the space for assembling the space state and more maneuverability are other advantages of these kinds of robot.

Some studies exist on determining MADL for different types of robotic systems. Determination of maximum allowable dynamic load for manipulators has applications in advanced trajectory planning, design and selection of robot manipulators. For instance, Thomas *et. al.* [1] used the load capacity as a criterion for sizing the actuator at the design stage of robotic manipulators and considered the maximum load in the neighborhood of a robot configuration. A technique was also developed in [2,3] to maximize the MADL of an entire trajectory, rather than in the neighborhood of a configuration. In these works, piece-wise rigid links and joints were assumed. Korayem and Basu [4-5] presented an algorithm for computing the MADL of elastic manipulators by relaxing the rigid body assumption. Yue *et. al.* [6] using a finite element method for describing the dynamics of a system, computed the maximum payload of kinematically redundant manipulators. Korayem and Ghariblu [7] developed an

1. *Professor, Dept. of Mech. Eng., Iran Univ. of Science and Tech., Tehran, Iran, Email: hkorayem@iust.ac.ir.*
2. *Ph.D. Candidate, Dept. of Mech. Eng., Iran Univ. of Science and Tech., Tehran, Iran.*
3. *Ph.D. Candidate, Dept. of Mech. Eng., Iran Univ. of Science and Tech., Tehran, Iran.*

algorithm for finding the MADL of rigid mobile manipulators. There are also some researches on carrying heavy loads or the application of large forces by mobile manipulators [8, 9]. Different types of constraints have been applied to a robotic system in order to solve the redundancy resolution [10, 11]. None of these published works considers finding the MADL on mobile manipulators using finite element approach including kinematic redundancy. The finite element method, which is a well-known powerful, modern computational tool, has been used almost universally during the past years to solve very complex structural engineering problems. One of the main advantages of FEM over most other approximate solution methods is the fact that FEM can handle irregular geometries routinely. Another significant advantage of FEM, especially over analytical solution techniques is the ease with which nonlinear conditions can be handled.

The main focus of this research is on mobile manipulators with the consideration of links elasticity. A brief introduction to the dynamics of these types of systems is being reviewed firstly. A strategy for determining the MADL subject to both constraints is described, where a series of ball-type bounds centered at the desired trajectory is used for defining the end-effector oscillation constraint, and motor speed-torque characteristics curve of a typical DC is used in the actuator constraint. A computational procedure is then presented, which allows computation of the MADL for an arbitrary prescribed dynamic motion of the end-effector. Finally, two numerical examples involving a two-link mobile manipulator considering the elasticity of links are presented and results are discussed.

MODEL DEVELOPMENT APPROACH

The overall approach involves treating each link of the manipulator as an assemblage of n_i elements of length l_i. For each of these elements the kinetic energy T_{ij} and potential energy V_{ij} are computed in terms of a selected system of n generalized variables $q = (q_1, q_2, \dots q_n)$, and their rate of change $\dot{q}$. These energies are then combined to obtain the total kinetic energy, T, and potential energy, V, for the entire system. For the sake of massive calculation, the above-mentioned procedure is presented in Appendix (A-1) to (A-3).

Dynamic equations for systems are derived through the Lagrange equations:

$$\frac{d}{dt}\left(\frac{\partial \mathcal{L}}{\partial \dot{q}_k}\right) - \frac{\partial \mathcal{L}}{\partial q_k} = Q_k, \qquad k = 1, 2, \dots n \tag{1}$$

where $\mathcal{L}$=T-V. Eq. (1) along with associated boundary conditions (Appendix (A-4)) provides the desired dynamic equations of the system as follows:

$$M\ddot{q} - f = Q \tag{2}$$

where $M = M(q)$ and $f = f(q, \dot{q})$ are nonlinear functions of generalized variables, q, and their rate of change, $\dot{q}$. Q denotes the applied torque at each joint.

DYNAMIC MODEL OF FLEXIBLE ROBOT MANIPULATOR

From Eqs. (A.9) and (A.20), the Lagrangian of link 1 is as follows:

$$\begin{aligned}\mathcal{L}_1 &= T_1 - V_1 \\ &= \frac{1}{2}\dot{q}_1^T M_1 \dot{q}_1 - m_1 g[0 \;\; 1] T_0^1 \begin{bmatrix} \frac{1}{2}n_1^2 l_1^2 \\ R_0 \psi_1 \end{bmatrix} - \frac{1}{2}\psi_1^T K_1 \psi_1.\end{aligned} \tag{3}$$

From Eqs. (A.17) and (A.23), the Lagrangian of link 2 can be derived:

$$\begin{aligned}\mathcal{L}_1 = \frac{1}{2}\dot{q}_2^T M_2 \dot{q}_2 - m_2 g[0 \;\; 1] T_0^1 \Bigg[\begin{bmatrix} L_1 \\ u_{2n_1+1} \end{bmatrix} n_2 l_2 \\ + T_1^2 \begin{bmatrix} \frac{1}{2}n_2^2 l_2^2 \\ R_1 \psi_2 \end{bmatrix} \Bigg] - \frac{1}{2}\psi_2^T K_2 \psi_2.\end{aligned} \tag{4}$$

The overall Lagrangian for a two-link flexible mobile manipulator with the base motion in x direction can then be written as:

$$\begin{aligned}\mathcal{L} &= \mathcal{L}_1(x_0, \theta_1, u_3, u_4, \dots u_{2n_1+2}) \\ &+ \mathcal{L}_2(x_0, \theta_1, u_{2n_1+1}, u_{2n_1+2}, \theta_2, w_3, w_4, \dots w_{2n_2+2})\end{aligned} \tag{5}$$

By applying Lagrange's equation (Eq. (1)) and performing some algebraic manipulations, the compact form of the system's dynamic equations becomes:

$$\sum_{j=1}^{n} M_{ij}\ddot{q}_j + \sum_{j=1}^{n}\sum_{k=1}^{n_j} h_{ijk}\dot{q}_j\dot{q}_k = R_i \;\; (i = 1, 2, .., n) \tag{6}$$

$$\sum_{j=1}^{n} M_{f,ij}\ddot{q}_j + \sum_{j=1}^{n}\sum_{k=1}^{n} h_{f,ijk}\dot{q}_j\dot{q}_k = R_{f,j} \tag{7}$$

where M, the inertia matrix, is comprised of element coefficients related with the second derivative of generalized variables, $\ddot{q}$. h considers the contribution of other dynamic forces such as centrifugal and Coriolis forces while R consists of gravity and other external forces. Dynamic Eqs. (6) and (7) are arranged on joint variables and deflections. To sum up Eq. (6) concerns the joints rotation in robot and Eq. (7) specifies the elastic deformation in links [7].

MODIFICATION OF THE MODEL TO INCLUDE A POINT MASS AT THE TIP AS LOAD

The extension of the model to a case where a point mass m_l is added at the tip of the manipulator can

be carried out following the proposed approach in the preceding section. For computing the kinetic and potential energies of the tip mass, the end-effector position $\vec{r}_m$ can be expressed as follows:

$$\vec{r}_m = \begin{Bmatrix} x_0 \\ 0 \end{Bmatrix} + T_0^1 \begin{bmatrix} L_1 \\ u_{2n_1+1} \end{bmatrix} + T_1^2 \begin{bmatrix} L_2 \\ u_{2n_2+1} \end{bmatrix} \quad (8)$$

After computing these energies, they can be added to the total energy of robot in Lagrange equation. One can show that the matrix differential model of the overall system in the matrix form, with manipulator at the tip is of the form:

$$M_T \ddot{q} - f_T = Q_T \quad (9)$$

where:

$$M_T = M + M_m,\ f_T = f + f_m,\ Q_T = Q + Q_m \quad (10)$$

and the subscript 'T' refers to the total system, and subscript 'm' represents the influence of the additional mass.

KINEMATIC MODEL OF FLEXIBLE ROBOT MANIPULATOR

Inverse kinematic can be used to derive the generalized variables (q) for a predefined trajectory which is useful in our following calculations for finding the MADL. If the vector of position of the end-effector is shown by $\vec{P} = X(q_r, q_f)^T$, then taking derivative with respect to time will yield the velocity of the end-effector:

$$\dot{\vec{P}} = [J_r, J_f](\dot{\vec{q}}_r, \dot{\vec{q}}_f)^T = J\,\dot{\vec{q}} \quad (11)$$

where q_r, q_f are generalized variables of joints rotation and deflection in links, respectively and J_f , J_r are the Jacobian matrices of the mobile robot manipulator for rigid and flexible generalized coordinates. After taking derivative of Eq. (11) with respect to time, equations of the end-effector's acceleration can be expressed as:

$$\ddot{\vec{P}} = [J_r, J_f](\ddot{\vec{q}}_r, \ddot{\vec{q}}_f)^T + [\dot{J}_r, \dot{J}_f](\dot{\vec{q}}_r, \dot{\vec{q}}_f)^T = J\,\ddot{\vec{q}} + \dot{J}\,\dot{\vec{q}} \quad (12)$$

Then by specifying the generalized coordinates of motion and their derivations, $\vec{q}, \dot{\vec{q}}, \ddot{\vec{q}}$ the geometrical coordinates of motion of the end-effector, $\vec{p}, \dot{\vec{p}}, \ddot{\vec{p}}$, can be obtained. On the contrary, in inverse kinematics if the trajectory of end-effector $(\vec{p}, \dot{\vec{p}}, \ddot{\vec{p}})$ is predefined, then the generalized coordinates of motion and their derivations $(\dot{\vec{q}}, \ddot{\vec{q}})$, can be specified. So, Eq. (12) can be rearranged in the following form:

$$\begin{aligned}(\ddot{\vec{q}}_r, \ddot{\vec{q}}_f)^T &= [J_r, J_f]^{-1}(\ddot{\vec{P}} - [\dot{J}_r, \dot{J}_f](\dot{\vec{q}}_r, \dot{\vec{q}}_f)^T) \\ &= J^{-1}(\ddot{\vec{P}} - \dot{J}\,\dot{\vec{q}}^T)\end{aligned} \quad (13)$$

In this case, the number of equations is less than the number of unknowns in Eq. (12); therefore, for inverting this equation and finding J^{-1} in Eq. (13) some additional equations are required as a complementary set. The first choice is dynamic equations that are governed on nodes of elements in FEM in the elastic link (Eq. (7)).

The resulting system of equations is not only highly coupled and nonlinear but also too lengthy which makes it extremely difficult to handle manually even for a low degree of freedom manipulator with a low number of elements.

FORMULATION OF MADL FOR A PREDEFINED TRAJECTORY

The MADL of a flexible link mobile manipulator is defined as the maximum load which the mobile manipulator can carry in performing the trajectory with acceptable precision for a pre-defined trajectory [7]. The emphasis on the tracking accuracy is due to relaxation of the rigid body assumption and to the fact that one of the main reasons for the deviation from the desired trajectory is the flexibility in links. This can be taken into account in MADL determination by imposing a constraint on the end-effector deflection, in addition to the actuator torque constraint. Deflection of the end-effector can cause excessive deflection from the pre-defined trajectory, even though the joint torque constraint is not violated. By considering the actuator torque and deflection constraints and adopting a logical computing method, the maximum load carrying capacity of a mobile manipulator for a given trajectory can be computed. The algorithm shown in Figure 1 is proposed for finding the MADL of the system.

This algorithm illustrates computing procedure for finding MADL with consideration of the manipulator workspace and end-effector trajectory. Due to the simultaneous motion of the vehicle and manipulator, the overall system has kinematic redundancy. Consequently kinematic equations system must be solved with the dynamic equations as a one equation set. Then, the actuator torque and end-effector deflection constraints must be checked for each point of the discretised trajectory. The associated MADL for the trajectory will be found. If this condition is fulfilled, the computed MADL will then be accepted as a final solution. The minimum value of this curve is specified as the maximum dynamic load that robot manipulator can carry within the defined conditions. Otherwise, the program jumps back to the first step and a new initial mass of load, m_l, must be selected until all constraints are satisfied.

Formulation of Actuator Torque Constraint

The joint actuator torque constraint was formulated based on the typical torque-speed characteristics of DC

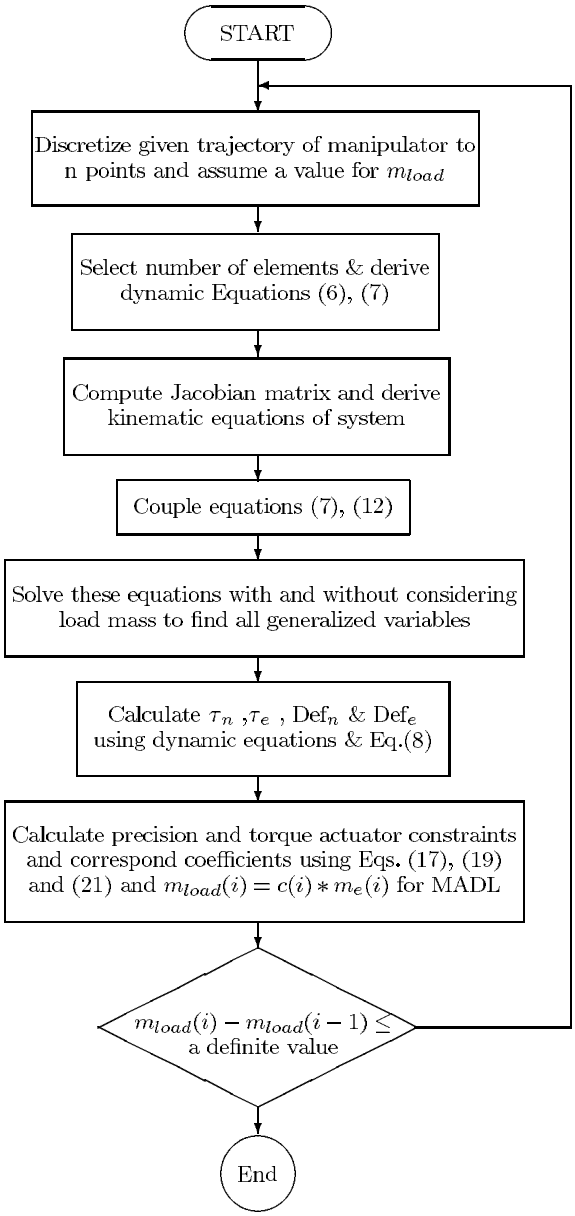

Figure 1. Flowchart of the computation procedure.

motors [7]. Other actuation systems can be dealt with similarly.

$$U^+ = k_1 - k_2\dot{q}$$

$$U^- = -k_1 - k_2\dot{q} \qquad (14)$$

where, $k_1 = T_s$, $k_2 = T_s\omega_{nl}$, T_s is the stall torque and ω_{nl} is the maximum no load speed of the motor. U^+ and U^- are the upper and lower bounds of the allowable torque. Using the computational procedure the ith joint torque due to the dynamics of a mobile vehicle and an n-link manipulator and load can be computed for each point of the discretised trajectory $(\tau_e)_i$, $i = 1, 2, \ldots, n + m$. Also, using Eq. (14) the upper and lower bounds of motor torques can be found and the available torque for the carrying load is then:

$$\tau_i^+ = (U^+)_i - (\tau_l)_i,$$

$$\tau_i^- = (U^-)_i - (\tau_l)_i. \qquad (15)$$

The maximum allowable torque at the ith joint is equal to:

$$\tau_i^+ = \max\{\tau_i^+, \tau_i^-\} \qquad (16)$$

Equation (16) remains valid for flexible manipulators because the linearity between the force F acting on the end-effector by the load mass and corresponding joint torques τ is preserved if small deformations are assumed. Therefore, it is necessary to introduce the concept of a load coefficient complying with the torque actuator constraint which can be calculated for each point of a given trajectory as follows:

$$(C_a)_j = \frac{|(\tau_{\max})_j - (\tau_{nl})_j|}{(\tau_l)_j} \qquad j = 1, 2, ..., m \qquad (17)$$

where τ_{nl} is the no-load torque. Physically, the load coefficient $(C_a)_j$ on the jth joint actuator describes the accessible torque for carrying the maximum load to the torque which is applied for carrying the initial load.

Formulation of Accuracy Constraint

Deflection at end-effector could be attributed to both static and dynamic factors, such as link flexibility, joint clearance, manipulator and load inertia. These factors are configuration dependent and for this, MADL varies from place to place on a given dynamic trajectory. A

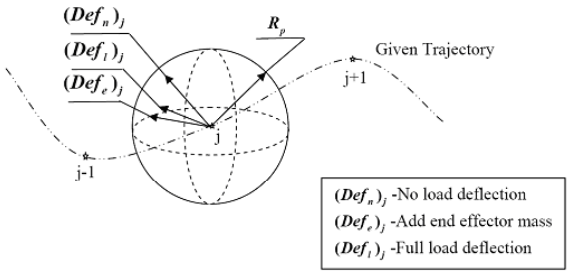

Figure 2. Spherical boundary of end-effector deflection [7].

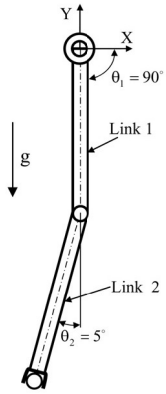

Figure 3. Initial condition for the simulation.

constraint should be imposed in such a way that the worst case, which corresponds to the least MADL, is used to determine the maximum allowable load.

A given trajectory is first digitized into manipulator points. No load deflection $(Def_n)_j$ and deflection with added end-effector mass $(Def_e)_j$ are calculated for $j = 1, 2, \ldots, m$, using the computational procedure outlined in appendix and Eq. (8). As seen in Figure 2, the additional mass at the end-effector changes both the magnitude and the direction of the deflection. But as long as the magnitude of the deflection is less or equal to an allowable value, the robot is considered to remain capable of executing the given trajectory. In other words, only the magnitude of deflection $(Def_n)_j$ and $(Def_e)_j$ need to be considered.

This prompted the use of a spherical boundary of radius R_p as the end-effector deflection constraint and the sphere is centered at the desired position on the

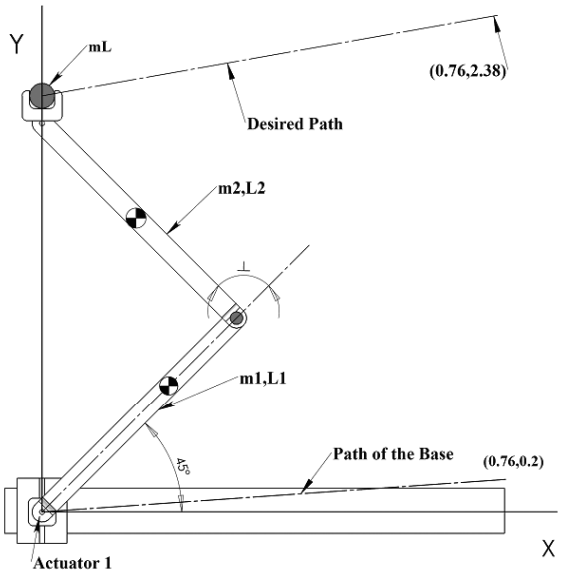

Figure 4. Schematic of robot and the desired path of end-effector.

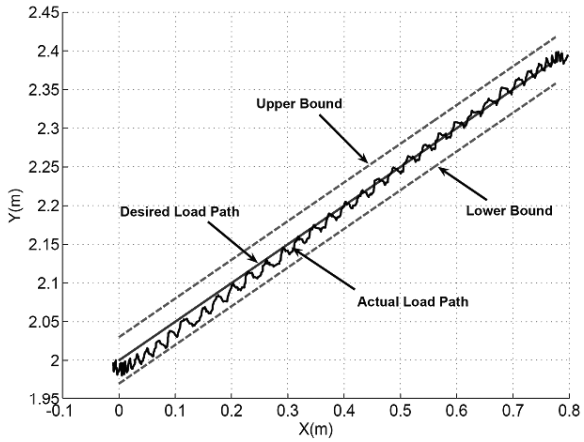

Figure 5. The desired and the actual load path.

given trajectory. Although $(Def_n)_j$ and $(Def_e)_j$ are generally vectors of different directions, the magnitude increases because the added mass at the end-effector is linearly related to the mass [7]. Therefore, the difference between the allowable deflection and the magnitude of deflection with added end-effector mass at point j is:

$$R_p - (Def_e)_j \tag{18}$$

which can be regarded as the remaining amount of end-effector deflection that can still be accommodated at point j of the given trajectory. This remaining amount indicates how much load can be carried through point j without violating the deflection constraint.

Therefore, it is necessary to introduce the concept of load coefficient $(C_a)_j$ for point j, $j = 1, 2, \ldots m$, as follows:

$$(C_a)_j = \frac{R_p - (Def_e)_j}{\max\{Def_e\} - \max\{Def_n\}} \tag{19}$$

where:

$$\max\{Def_e\} = \max\{(Def_e)_1, (Def_e)_2, ..., (Def_e)_m\}$$
$$\max\{Def_n\} = \max\{(Def_n)_1, (Def_n)_2, ..., (Def_n)_m\}. \tag{20}$$

Finally the load coefficient (c) can be obtained as follows:

$$c = \min\{(C_p)_j, (C_a)_j\}, \quad j = 1, 2, ..., m. \tag{21}$$

Then, the maximum mass that can be carried on the given trajectory is $m_{load} = c \times m_e$.

SIMULATION RESULTS AND DISCUSSION

In order to initially check the validity of the presented model, the response of the system, with a very large elastic constant (EI), to an initial conditions corresponding to θ_1= -90 deg and θ_2= 5 deg (Figure 3) is simulated. The response of the system is in agreement with the harmonic motion of an inelastic bar hanging freely under gravity. Once more, this problem is performed for a robot manipulator with elastic links. The results are in very good accord with a similar case in paper of Usoro *et. al.* [12].

Two additional simulations of the system are performed. In the first test, a robot manipulator with

Table 1. Simulation of Parameters

Parameter	Value	Unit
Length of Links	L_1=L_2=1.414	m
Mass	m_1=0.7, m_2=0.5	Kg
Moment of Inertia	I_1=I_2=5.5e-4	Kg.m^2
Spring Constant	K_1=15, K_2=10	N.m
Actuator Stall Torque	Ks_1=18,Ks_2=25	Nm.s/rad

elastic links is considered. The end-effector and its load must track a straight line with a predefined speed. In the second test, MADL is found for a flexible robot manipulator in which end-effector must move along a circular path. In both cases, the mobile base of manipulator moves along a straight line with a constant speed.

Test 1: MADL of a Flexible Mobile Robot Manipulator with a Linear Path of End-effector

This simulation study is performed to investigate the efficiency of the procedure presented in Figure 1, for computing the maximum allowable load of a mobile manipulator. All required parameters are given in Table 1.

As it was mentioned earlier, the path of end-effector and its payload is linear and starts from point $(x_1 = 0, y_1 = 2m)$ and ends at a point with coordinate $(x_2 = 0.76m, y_2 = 2.38m)$ (Figure 4). The velocity

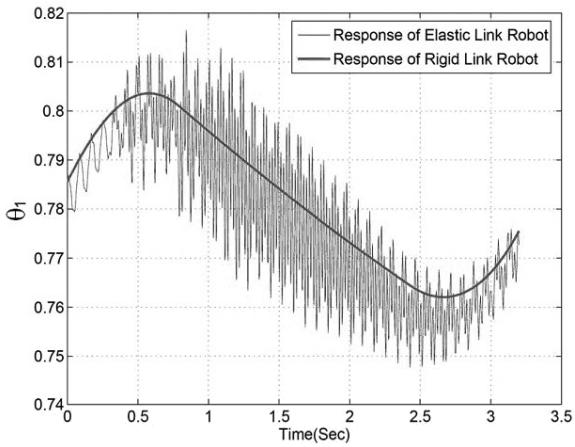

Figure 6. Joint responses of θ_1 for rigid and flexible links.

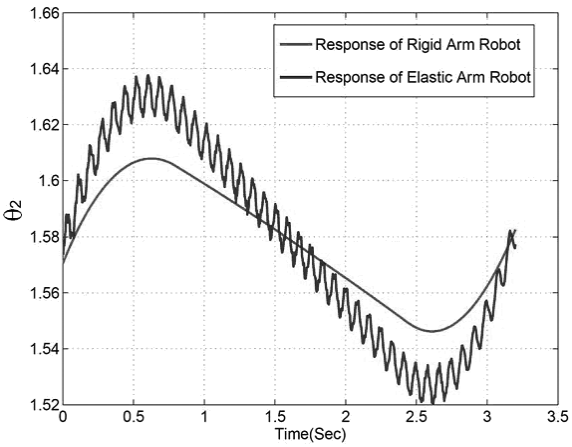

Figure 7. Joint responses of θ_2 for rigid and flexible links.

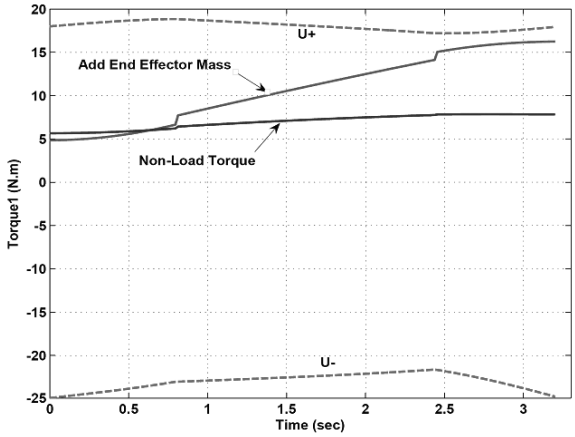

Figure 8. Applied torques of the first motor.

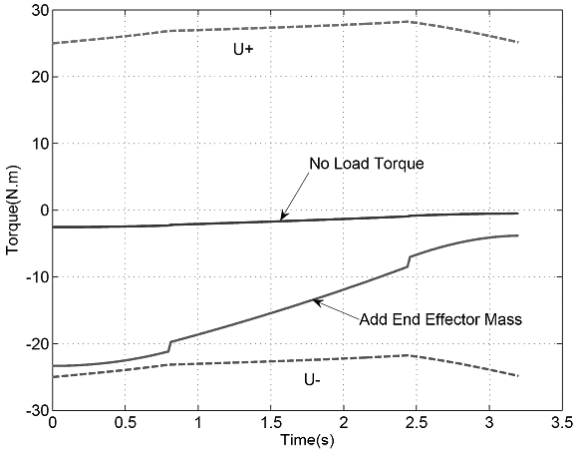

Figure 9. Applied torques of the second motor.

profile of the end-effector is as below:

$$\begin{cases} v = a\,t & 0 \le t \le T/4 \\ v = v_{\max} & T/4 \le t \le 3T/4 \\ v = -a\,t & 3T/4 \le t \le T \end{cases} \tag{22}$$

The permissible error bound for the load motion around the desired path is limited to $Re = 0.03m$. To find a suitable base trajectory, initially a linear path is selected for the vehicle, which starts from a point with coordinate $(x_{b1} = 0m, y_{b1} = 0m)$ and ends at $(x_{b2} = 0.2m, y_{b2} = 0.2m)$. The obtained path of the end-effector, considering link flexibility is shown in Figure 5 in comparison with the desired path. Also the joint angles of rigid and flexible links are shown in Figures 6 and 7. The corresponding applied torques to the vehicle and manipulator actuators for the final path of the vehicle are shown in Figures 8 and 9. Finally Figure 10 shows the equivalent MADL at each instant for the final motion.

Test 2: MADL of a Flexible Mobile Robot Manipulator with a Circular Path of End-effector

In this simulation, the computation of the MADL for a two-link planar manipulator mounted on an XY table

(Figure 11) is presented. The link parameters and inertia properties of the manipulator were given in Table 2. In the inertial reference frame, the XY table is capable of moving 1000 mm along the X-axis and 200 mm along the Y-axis. Base velocity is $V_x = 0.5$t. Also, it is assumed that the load must move along a circular path. The centre of the circular path coordinates with a radius r = 50cm, is at $(x_c = 1m; y_c = 1m)$ with origin at the lower-left corner of the XY table (Figure 12). The angular velocity of the end-effector is 180 deg/s with an overall time of the motion 1.5 s. With this initial condition (given time and angular velocity) only 3/4 of a full circle will be tracked.

The base work space (BWS) was discretised into 20 equal distance points in both traversing directions and into 40 points in the load trajectory. The maximum allowable error-bound at each point of the desired path must lie on a sphere with the radius of 5 cm.

The obtained path which is tracked with the flexible robot manipulator was compared with the desired path and is shown in Figure 12. The graph shows that, the accuracy constraint is violated between $t = 0.8s$ and $t = 1.38s$. It can be concluded that the assumed value for m_{load} is more than the robot allowable dynamic load and so another value for m_{load} must be chosen. After correcting this value, the obtained load trajectory satisfies the precision constraint.

Joint angles of rigid and flexible links were shown in Figures 13 and 14, for the final motion. The

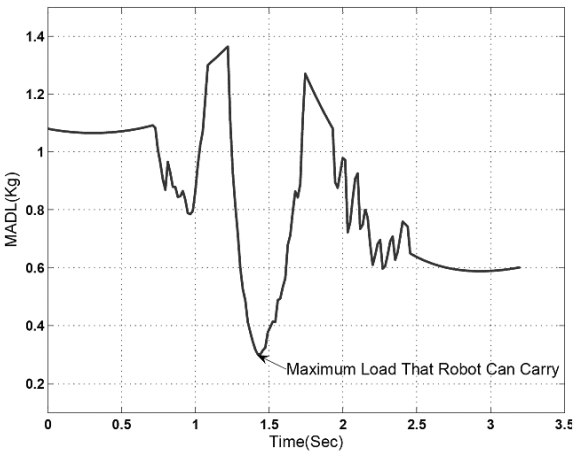

Figure 10. Maximum Allowable Dynamic Load (MADL).

Table 2. Link parameters and inertia properties of two-arm planar flexible manipulator.

Parameter	Value	Unit
Length of Links	L_1=L_2=1.2	m
Mass	m_1=0.80, m_2=0.80	Kg
Moment of Inertia	I_1=I_2=5.5e-4	Kg.m^2
Spring Constant	K_1=17, K_2=12	N.m
Actuator Stall Torque	Ks_1=12,Ks_2=30	Nm.s/rad

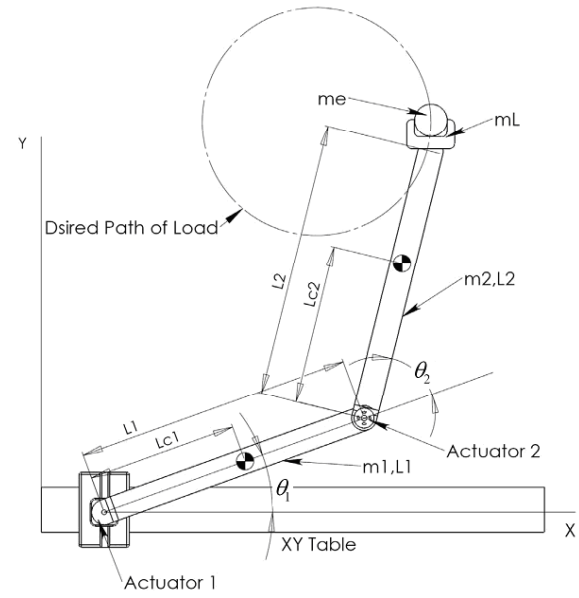

(a)

(b)

Figure 11. Schematic view of the flexible link planar manipulator with mobile base.

equivalent MADL at the each instant of time is shown in Figure 15. In this case, the maximum dynamic load is found to be equal to 0.54 kg.

CONCLUSIONS

The main objective of this study was to formulate the MADL and determining the "maximum load" for flexible-link manipulators with a pre-defined trajectory, using the finite element method. This was achieved by imposing actuator torque capacity and end-effector deformation constraints upon the problem formulation.

In these simulation studies, a two arm planar manipulator mounted on a mobile base is considered for carrying a load on two predefined trajectories and is examined in two test cases.

In the first case, none of the joint motors is required to move at its full capacity until just before t=2.5 s, whose torque in joint 1 increases and ap-

proaches the upper bound (Figure 8). It can be concluded that actuator torque capacity is the dominant constraint for determining the maximum allowable load of the motion because the elastic trajectory is almost far from the bounds in Figure 5, and precision constraint is not a determiner in this case then.

Another point is that, the response of the first joint (Figure 6) is oscillating around the response of inelastic-link system, but response of the second joint is less oscillatory and a bit far from the response of the rigid state. Presence of deviation in θ_2 from inelastic state in comparison with θ_1 is because of the elasticity in the first link and consequently gathering some accumulative errors at the end of this link. The motion of the second link is disturbed by these errors, which in turn increase the amplitude of oscillation (Figure 7). Lesser frequency for response in joint 2 is because of smaller inertia in this joint.

In the second case, the maximum dynamic load is determined to be 0.54 kg in $t = 0.9s$. In the first attempt, the accuracy of the end-effector is violated (Figure 12). As mentioned in the procedure for finding

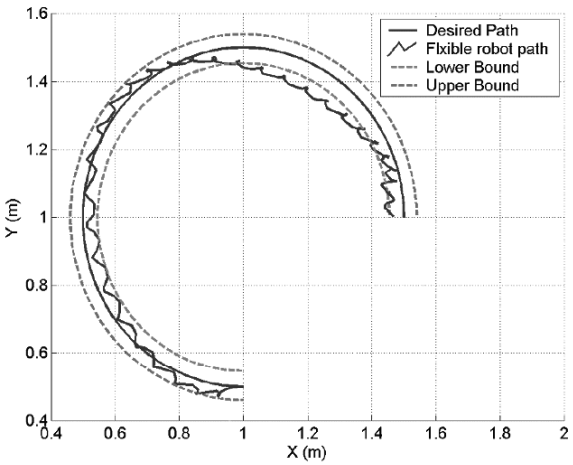

Figure 12. Comparison of flexible joint robot path with respect to desired path.

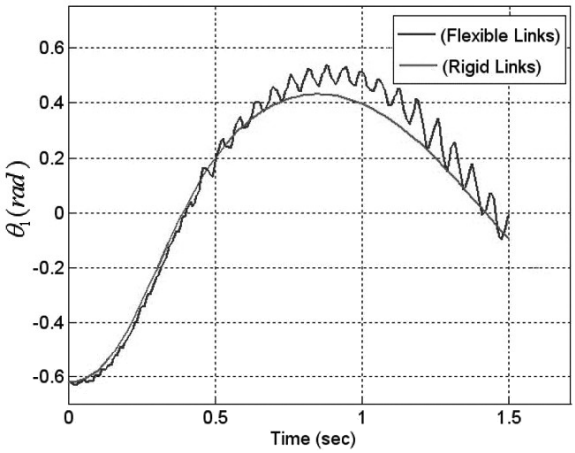

Figure 13. Joint responses of $theta_1$ for Rigid and flexible Links.

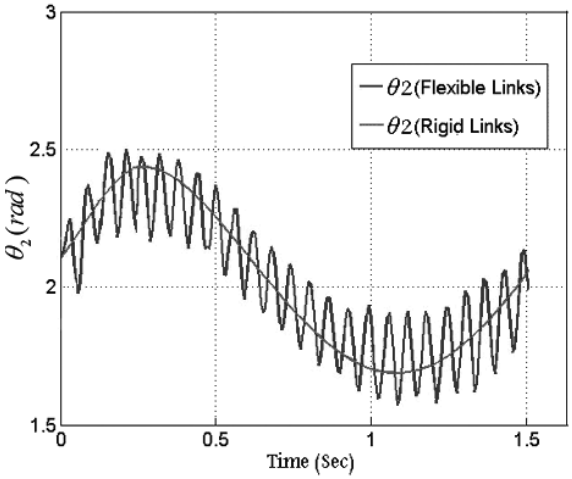

Figure 14. Joint responses of θ_2 for Rigid and flexible Links.

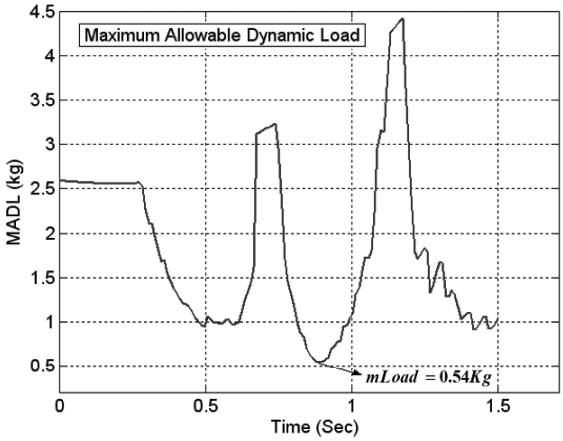

Figure 15. Maximum allowable dynamic load.

the MADL, either m_{load} can be modified in the second try or the base trajectory can be changed without changing the end-effector trajectory. Therefore, in the mobile base manipulator there is a better chance for carrying more loads in comparison to fixed base robots.

APPENDIX

A-1: Model Development for a Two-Link Manipulator

Consider a two-link flexible manipulator as depicted in Figure 16 The mobile base can move in XY plane, but for the sake of simplicity and avoiding massive computations only the motion in x direction is considered as the only degree of freedom of the base in the following computations.

Consider link 1 to be divided into elements '11','12',...,'1j',..., '1n_1' of equal length l_1, and link 2 to be divided into elements '21','22',...,'2j',...,'2n_2' of equal length l_2. Let us define the following notation where subscript i refers to link i, and subscript ij refers to the jth element of link i:

OXY is the inertia system of coordinates, $O_iX_iY_i$ is body-fixed system of coordinates attached to link i.

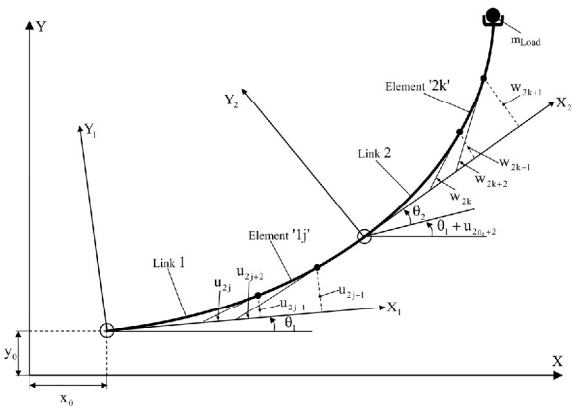

Figure 16. Schematic of a two-link flexible mobile manipulator.

u_{2j-1} flexural displacement at the common junction of elements $1(j-1)$ and $1j$ of link 1. u_{2j} flexural slope at the tip of common junction of elements '$1(j-1)$' and '$1j$' of link 1. This slope is measured with respect to axis O_1X_1. w_{2j-1}, w_{2j} flexural displacement and slope at the common junction of elements '$2(j-1)$' and '$2j$' of link 2. This slope is measured with respect to axis O_2X_2 and n_1, n_2 are the numbers of elements of links 1 and 2, respectively.

A-2: Kinetic Energy Computation

Kinetic Energy for an Element '1j' of Link 1

The kinetic energy T_{1j} for the jth element of link 1 may be computed as:

$$T_{1j} = \frac{1}{2}\int_0^{l_1} m_1 \left[\frac{\partial r^T}{\partial t}.\frac{\partial r}{\partial t}\right] dx_{1j} \qquad (A.1)$$

It is convenient to express the vector $\vec{r}$, in terms of a vector $\vec{r}_1$ in the body-fixed system of coordinates $O_1X_1Y_1$ and $\vec{r}_0$ in inertia reference frame.

$$\vec{r} = \vec{r}_0 + T_0^1\,\vec{r}_1 \qquad (A.2)$$

where $\vec{r}_0 = \begin{Bmatrix} x_0 \\ 0 \end{Bmatrix}, \vec{r}_1 = \begin{bmatrix} (j-1)l_1 + x_{1j} \\ y_{1j} \end{bmatrix}, T_0^1 = \begin{bmatrix} \cos\theta_1 & -\sin\theta_1 \\ \sin\theta_1 & \cos\theta_1 \end{bmatrix}$ and θ_1 is the joint angle between O_1X_1 and OX. The displacement y_{1j} can be described in terms of shape functions of a beam element $\phi_k(x_{1j})$ as:

$$y_{1j}(x_{1j},t) = \sum_{k=1}^{4} \phi_k(x_{1j})\, u_{2j-2+k}(t) \qquad (A.3)$$

$\phi_k(x_{1j})$ can be found in FEM context. From Eqs. (A.2) and (A.3), we have:

$$\frac{\partial r^T}{\partial t}.\frac{\partial r}{\partial t} = \dot{z}_j^T \begin{bmatrix} \left[\frac{\partial r}{\partial x_0}\right]^T \\ \left[\frac{\partial r}{\partial \theta_1}\right]^T \\ \left[\frac{\partial r}{\partial u_{2j-1}}\right]^T \\ \vdots \\ \left[\frac{\partial r}{\partial u_{2j+2}}\right]^T \end{bmatrix} \begin{bmatrix} \frac{\partial r}{\partial x_0} & \frac{\partial r}{\partial \theta_1} & \frac{\partial r}{\partial u_{2j-1}} & \cdots \frac{\partial r}{\partial u_{2j+2}} \end{bmatrix} \dot{z}_j \qquad (A.4)$$

where $z_j = [x_0\ \theta_1\ u_{2j-1}\ u_{2j}\ u_{2j+1}\ u_{2j+2}]^T$. Thus, from Eqs. (A.1) to (A.4), the kinetic energy T_{1j} of element '$1j$' may be expressed as:

$$T_{1j} = \frac{1}{2}\dot{z}_j^T M_{1j} \dot{z}_j \qquad (A.5)$$

where

$$M_{1j}(i,k) = \int_0^{l_1} m_1 \left(\frac{\partial \vec{r}}{\partial z_{ji}}\right)^T \frac{\partial \vec{r}}{\partial z_{jk}}\, dx_{1j}\,, \quad i,k = 1,2,...,6 \qquad (A.6)$$

and z_{ji} is the ith element of z_j. It can be shown that M_{1j} is:

$$M_{1j} = \begin{bmatrix} M_{1j}(1,1) & M_{1j}(1,2) & \cdots & M_{1j}(1,6) \\ M_{1j}(2,1) & M_{1j}(2,2) & \cdots & M_{1j}(2,6) \\ \vdots & \vdots & & \\ M_{1j}(6,1) & M_{1j}(6,2) & & P_{ij} \end{bmatrix} \qquad (A.7)$$

where P_{ij} is the general mass matrix of beam element which can be found in FEM contexts. Other elements of M_{1j} can be calculated using Eq. (A.6) as follows:

$$M_{1j}(1,1) = m_1 L_1$$

$$M_{1j}(1,2) = m_1\left(-\frac{l_1^2}{2} - (j-1)\,l_1^2\right)\sin\theta_1 - m_1\cos\theta_1 \vec{\psi}_{1j}\begin{bmatrix} \frac{l_1}{2} & \frac{l_1^2}{12} & \frac{l_1}{2} & -\frac{l_1^2}{12} \end{bmatrix}^T \qquad (A.8)$$

with $\psi_{1j} = [u_{2j-1}\ u_{2j}\ u_{2j+1}\ u_{2j+2}]$. Other elements of M_{1j} can be found completely in [13].

Total Kinetic Energy of Link 1
As link 1 is divided into n_1 elements, the total kinetic energy of link 1 is computed by adding the overall elements '1j' of link 1,

$$T_1 = \sum_{j=1}^{n_1} T_{1j} = \sum_{j=1}^{n_1} \frac{1}{2} \dot{z}_j^T M_{1j} \dot{z}_j = \frac{1}{2} \dot{\tilde{q}}_1^T \tilde{M}_1 \dot{\tilde{q}}_1 \qquad (A.9)$$

where:

$$\tilde{q}_1 = [x_0, \theta_1, \tilde{\psi}_1^T]^T,$$

$$\tilde{\psi}_1 = [u_1 \; u_2 \; u_3 \; u_4 \; \cdots \; u_{2n_1-1} \; u_{2n_1} \; u_{2n_1+1} \; u_{2n_1+2}]^T \qquad (A.10)$$

$\tilde{M}$ is a generalized inertia matrix that is assembled from n mass matrices of n elements for link 1.

Kinetic Energy for an Element '2j' of Link 2
The kinetic energy T_{2j} for jth element of link 2 may be computed using Eqs. (A.5) and (A.6) by considering an appropriate $\vec{r}$ vector as below:

$$\vec{r} = \begin{Bmatrix} x_0 \\ 0 \end{Bmatrix} + T_0^1 \begin{bmatrix} L_1 \\ u_{2n_1+1} \end{bmatrix} + T_1^2 \begin{bmatrix} (j-1)l_2 \\ y_{2j} \end{bmatrix} \qquad (A.11)$$

where T_0^1 was described in Eq. (A.2). T_1^2 is the transformation matrix between the body-fixed system of coordinates, $O_1X_1Y_1$ and $O_2X_2Y_2$ which is attached to the first and the second links with angle of $\theta_2 + u_{2n1+2}$, (Figure 16) and y_{2j} may be computed as:

$$y_{2j}(x,t) = \sum_{i=4}^{4} \phi_i(x) \, W_{2j-2+i}(t), \qquad (A.12)$$

From Eqs. (A.11) to (A.12), it can be concluded that $\vec{r}$ is independent of u_i for $i = 1, 2, \ldots, 2n_1$. With mathematical simplifications and the assumption that $q = \theta_2 + u_{2n_1+2}$ and using extended transformation matrix, the position of each point on jth element in the second link can be written as:

$$\vec{r} = \begin{bmatrix} \cos(\theta_1+q) & -\sin(q+\theta_1) & x_0 \\ \sin(q+\theta_1) & \cos(q+\theta_1) & 0 \\ 0 & 0 & 1 \end{bmatrix} \begin{bmatrix} (j-1)l_2+x_{2j} \\ y_{2j} \\ 1 \end{bmatrix} + \begin{bmatrix} L_1 \cos\theta_1 - u_{2n_1+1} \sin\theta_1 \\ L_1 \sin\theta_1 + u_{2n_1+1} \cos\theta_1 \\ 0 \end{bmatrix} \qquad (A.13)$$

Then, T_{2j} in Eq. (A.5) may be expressed as:

$$T_{2j} = \frac{1}{2} \dot{z}_j^T M_{2j} \dot{z}_j, \qquad (A.14)$$

where

$$z_j^T = [x_0 \; \theta_1 \; u_{2n_1+1} \; u_{2n_1+2} \; \theta_2 \; \psi_{2j}^T],$$

and

$$\psi_{2j}^T = [w_{2j-1} \; w_{2j} \; w_{2j+1} \; w_{2j+2}]. \qquad (A.15)$$

Hence, the mass matrix M_{2j} is a (9×9) matrix whose elements can be routinely computed by the following equation:

$$M_{2j}(i,k) = m_2 \int_0^{l_2} \left[\frac{\partial \vec{r}}{\partial z_{ji}} \right]^T \frac{\partial \vec{r}}{\partial z_{jk}} \, dx_{2j} \qquad i, k = 1, 2, ..., 9 \qquad (A.16)$$

where z_{ji} is the ith element of z_j.

Total Kinetic Energy for Link 2
The kinetic energy T_2 for link 2 is computed by summing over all elements '2j' of link 2, *i.e.*,

$$T_2 = \sum_{j=1}^{n_2} T_{2j} = \sum_{j=1}^{n_2} \frac{1}{2} \dot{z}_j M_{2j} \dot{z}_j = \frac{1}{2} \dot{\tilde{q}}_2^T \tilde{M}_2 \dot{\tilde{q}}_2 \qquad (A.17)$$

where $\tilde{q}_2 = [x_0 \; \theta_1 \; u_{2n_1+1} \; u_{2n_1+1} \; \theta_2 \; \tilde{\psi}_2^T]^T$, and $\tilde{\psi}_2 = [w_1 \; w_2 \; ... \; w_{2n_2+1} \; w_{2n_2+2}]^T$.

A-3: Potential Energy Computation
The potential energy for the overall system is obtained by computing the potential energy for each element of the assemblage and adding up all the elements.

Potential Energy for a Single Element '1j' of Link1
Considering OX as the reference, the potential energy V_{1j} of element '1j' of link 1 comprises two components, V_{g1j} due to gravity and V_{e1j} due to elasticity. Considering that the mobility in x_0 direction does not have any effects on V_{1j}, the potential energy of element '1j' of link 1 becomes:

$$V_{1j} = V_{g1j} + V_{e1j} = \int_0^{l_1} m_1 g \, [0 \; 1] \, T_0^1 \begin{bmatrix} (j-1)\, l_1 + x_{1j} \\ y_{1j} \end{bmatrix} dx_{1j} + \frac{1}{2} \int_0^{l_1} E I_1 \left[\frac{\partial^2 y_{1j}}{\partial x_{1j}^2} \right]^2 dx_{1j} \qquad (A.18)$$

By substituting for y_{1j} from Eq. (A.3) and taking integration with respect to time, the elemental potential energy becomes:

$$V_{1j} = \frac{1}{2} \psi_{1j}^T k_{1j} \psi_{1j} + m_1 g \, [0 \; 1] T_0^1 \begin{bmatrix} (j-\frac{1}{2}) l_1^2 \\ \frac{l_1}{2} u_{2j-1} + \frac{l_1^2}{12} u_{2j} + \frac{l_1}{2} u_{2j+1} - \frac{l_1^2}{12} u_{2j+2} \end{bmatrix} \qquad (A.19)$$

where ψ_{1j} is defined in (A.8), and K_{1j} is stiffness matrix of beam element.

Total Potential Energy for Link 1
Since link 1 comprises n_1 elements, its total potential energy is:

$$V_1 = \sum_{j=1}^{n_1} V_{1j} = m_1 g [0\ \ 1] T_0^1 \begin{bmatrix} \frac{1}{2} n_1^2 l_1^2 \\ R_0 \tilde{\psi}_1 \end{bmatrix} + \frac{1}{2} \tilde{\psi}_1^T \tilde{K}_1 \tilde{\psi}_1 \qquad (A.20)$$

where $\tilde{\psi}_1$ is defined in Eq. (A.10) and R_0 is obtained as follow:

$$\text{for } n_1 = 1, \quad R_0 = \begin{bmatrix} \frac{l_1}{2} & \frac{l_1^2}{12} & \frac{l_1}{2} & \frac{-l_1^2}{12} \end{bmatrix}$$

$$\text{for } n_1 = 2, \quad R_0 = \begin{bmatrix} \frac{l_1}{2} & \frac{l_1^2}{12} & l_1 & 0 & \frac{l_1}{2} & \frac{-l_1^2}{12} \end{bmatrix}$$

$$\text{for } n_1 = 3, \quad R_0 = \begin{bmatrix} \frac{l_1}{2} & \frac{l_1^2}{12} & l_1 & 0 & l_1 & 0 & \frac{l_1}{2} & \frac{-l_1^2}{12} \end{bmatrix} \qquad (A.21)$$

Elements of $\tilde{K}$, the general stiffness matrix can be found in [13].

Potential Energy for a Single Element '2j'
Considering again OX as the reference, the potential energy V_{2j} of the jth element of link 2 is the sum of two components. One is due to gravity and the other due to elasticity of the system, *i.e.*

$$\begin{aligned} V_{2j} =& \int_0^{l_2} m_2 g [0\ \ 1] \left[T_0^1 \begin{bmatrix} L_1 \\ u_{2n_1+1} \end{bmatrix} \right. \\ & \left. + T_0^1 T_1^2 \begin{bmatrix} (j-1) l_2 + x_{2j} \\ y_{2j} \end{bmatrix} \right] dx_{2j} \\ & + \frac{1}{2} \int_0^{l_2} EI_2 \left[\frac{\partial^2 y_{2j}}{\partial x_{2j}^2} \right]^2 dx_{2j} \\ & = m_2 g [0\ \ 1] \left[T_0^1 \begin{bmatrix} L_1 \\ u_{2n_1+1} \end{bmatrix} l_2 \right. \\ & \left. + T_0^1 T_1^2 \begin{bmatrix} (j - \frac{1}{2}) l_2^2 \\ \frac{l_2}{2} w_{2j-1} + \frac{l_2^2}{12} w_{2j} + \frac{l_2}{2} w_{2j+1} - \frac{l_2^2}{2} w_{2j+2} \end{bmatrix} \right] \\ & + \frac{1}{2}\ \psi_{2j}^T K_{2j} \psi_{2j} \qquad (A.22) \end{aligned}$$

where ψ_{2j} is given in Eq. (A.15).

Total Potential Energy for Link 2
Summing up all elements '2j' of Link 2, the total potential energy of this link becomes:

$$V_2 = \sum_{j=1}^{n_2} V_{2j} = m_2 g [0\ \ 1] \left[T_0^1 \begin{bmatrix} L_1 \\ u_{2n+1} \end{bmatrix} n_2 l_2 + T_0^1 T_1^2 \begin{bmatrix} \frac{1}{2} n_2^2 l_2^2 \\ R_1 \psi_2 \end{bmatrix} \right] + \frac{1}{2} \tilde{\psi}_2^T K_2 \tilde{\psi}_2 \qquad (A.23)$$

where $\tilde{\psi}_2 = [w_1\ \ w_2\ \ \cdots\ \ w_{2n_2+2}]$ and, R_1 is obtained of Eq. (A.21) by replacing l_2 instead of l_1. The elements of $\tilde{K}_2$ can be found in [13].

A-4: Boundary Condition
In this simulation, it is assumed that first joint of link 1 is constrained to have no displacement or angular displacement due to body-fixed axis O_1X_1. It means that, boundary variables u_1 and u_2 must be zero *i.e.* $u_1(t) = 0$ and $u_2(t) = 0$. First joint in link 2 has similar constraints and has no displacement or angular displacement due to O_2X_2. Hence, constraint variables w_1 and w_2 must be zero *i.e.* $w_1(t) = 0$ and $w_2(t) = 0$. It must be considered that both links have angular displacements θ_1 and θ_2 with thier body-fixed axis.

REFERENCES

1. Thomas M., Yuan-Chou HC., Tesar D., "Optimal Actuator Sizing for Robotic Manipulators Based on Local Dynamic Criteria", *J. of Mechanisms Transmission Automation in Design*, **107**, PP 163-169(1985).
2. Wang L.T., Ravani B., "Dynamic Load Carrying Capacity of Mechanical Manipulators", *J. of Dynamic System Measurement Control*, **110**, PP 46-52(1988).
3. Wang L.T., Ravani B., "Dynamic Load Carrying Capacity of Mechanical Manipulators, Part II, computational procedure and applications", *J. of Dynamic System Measurement Control*, **110**, PP 53-61(1988).
4. Korayem M. H., Basu A., "Formulation and Numerical Solution of Elastic Robot Dynamic Motion with Maximum Load Carrying Capacity", *J. of Robotica*, **12**, PP 253-261(1994).
5. Korayem M. H., Basu A., "Dynamic Load Carrying Capacity for Robotic Manipulators with Joint Elasticity Imposing Accuracy Constraints", *J. of Robotic and Autonomous Systems*, **13**(219-229), (1994).
6. Yue S., Tso S. K., Xu W. L., "Maximum Dynamic Payload Trajectory for Flexible Robot Manipulators with Kinematic Redundancy", *Mechanism and Machine theory*, **36**, PP 785-800(2001).
7. Korayem M. H., Ghariblu H., "Maximum Allowable Load on Wheeled Mobile Manipulators Imposing Redundancy Constraints", *J. of Robotic and Autonomous Systems*, **44**(2), PP 151-159(2003).
8. Rey D. A., Papadopoulos E. G., "Online Automatic Tip-Over Presentation for Mobile and Redundant Manipulators", *Proc. of the IEEE International Conference on Intelligent Robots and Systems (IROS97)*, PP 1273-1278(1997).
9. Papadopoulos E., Gonthier Y., "A Frame Force For Large Force Task Planning of Mobile and Redundant Manipulators", *J. of Robot System*, **16**(3), PP 151-162(1999).
10. Seraji H., "A Unified Approach to Motion Control of Mobile Manipulators", *J. of Robot Research*, **17**(12), PP 107-118(1998).
11. Chung P. H., "An Extension to Operational Space for Kinematically Redundant Manipulators: Kinematics and Dynamics", *IEEE International Conference on Robotics and Automation*, **16**(5), PP 592-596(2000).

12. Usoro P. B., Nadira R., Mahil, "A Finite Element-Lagrange Approach to Modeling Lightweight Flexible Manipulators", *Journal of Dynamic Systems, Measurement, and Control*, **108**, PP 198-205(1986).

13. A. Heidari, "Maximum dynamic Load Carrying Capacity for Flexible Robot Manipulators with Finite Element Approach", M.Sc. Thesis, Faculty of Mechanical Engineering, Science and Technology University(2005).